doi:10.1093/brain/awaa017 BRAIN 2020: 143; 833–843 | 833

BRAIN
A JOURNAL OF NEUROLOGY

Dynamics of recovery from anaesthesia-induced unconsciousness across primate neocortex

Shaun R. Patel,[1] Jesus J. Ballesteros,[2] Omar J. Ahmed,[3] Pamela Huang,[4] Jessica Briscoe,[1] Emad N. Eskandar[5] and Yumiko Ishizawa[2]

How the brain recovers from general anaesthesia is poorly understood. Neurocognitive problems during anaesthesia recovery are associated with an increase in morbidity and mortality in patients. We studied intracortical neuronal dynamics during transitions from propofol-induced unconsciousness into consciousness by directly recording local field potentials and single neuron activity in a functionally and anatomically interconnecting somatosensory (S1, S2) and ventral premotor (PMv) network in primates. Macaque monkeys were trained for a behavioural task designed to determine trial-by-trial alertness and neuronal response to tactile and auditory stimulation. We found that neuronal dynamics were dissociated between S1 and higher-order PMv prior to return of consciousness. The return of consciousness was distinguishable by a distinctive return of interregionally coherent beta oscillations and disruption of the slow-delta oscillations. Clustering analysis demonstrated that these state transitions between wakefulness and unconsciousness were rapid and unstable. In contrast, return of pre-anaesthetic task performance was observed with a gradual increase in the coherent beta oscillations. We also found that recovery end points significantly varied intra-individually across sessions, as compared to a rather consistent loss of consciousness time. Recovery of single neuron multisensory responses appeared to be associated with the time of full performance recovery rather than the length of recovery time. Similar to loss of consciousness, return of consciousness was identified with an abrupt shift of dynamics and the regions were dissociated temporarily during the transition. However, the actual dynamics change during return of consciousness is not simply an inverse of loss of consciousness, suggesting a unique process.

1 Department of Neurology, Massachusetts General Hospital, Harvard Medical School, Boston MA, USA
2 Department of Anesthesia, Critical Care and Pain Medicine, Massachusetts General Hospital, Harvard Medical School, Boston MA, USA
3 Departments of Psychology, Neuroscience and Biomedical Engineering, University of Michigan, Ann Arbor MI, USA
4 Department of Anesthesia and Perioperative Care, University of California San Francisco, San Francisco CA, USA
5 Departments of Neurological Surgery, Neuroscience, Psychiatry and Behavioral Sciences, Albert Einstein College of Medicine, Bronx NY, USA

Correspondence to: Yumiko Ishizawa
Department of Anesthesia, Critical Care and Pain Medicine, Massachusetts General Hospital,
Harvard Medical School, Boston MA, USA
E-mail: yishizawa@mgh.harvard.edu

Keywords: general anaesthesia; return of consciousness; sensory premotor network; local field potentials; non-human primates

Abbreviations: LOC = loss of consciousness; LFP = local field potential; PMv = ventral premotor area; ROC = return of consciousness; ROPAP = return of pre-anaesthetic performance

Received December 13, 2018. Revised October 7, 2019. Accepted December 8, 2019. Advance Access publication February 12, 2020

Introduction

How our brain recovers from general anaesthesia is poorly understood. Emergence and postoperative neurocognitive problems affect patients of all ages undergoing surgery (Lepouse *et al.*, 2006; Vlajkovic and Sindjelic, 2007; Monk and Price, 2011) and are associated with an overall increase in morbidity and mortality (Monk *et al.*, 2008; Steinmetz *et al.*, 2009; Witlox *et al.*, 2010). The mechanisms of neurocognitive problems following general anaesthesia are not well understood (Monk *et al.*, 2008; Steinmetz *et al.*, 2009; Witlox *et al.*, 2010) and the role of anaesthetic agents is unclear. Despite its importance, animal models are scarce (Cibelli *et al.*, 2010; Stratmann *et al.*, 2010; Carr *et al.*, 2011). Elucidating the mechanisms of neural recovery from general anaesthesia is an essential first step in understanding these potentially detrimental complications in patients.

Human EEG studies suggest that return of consciousness (ROC) from general anaesthesia is an inverse process of loss of consciousness (LOC) (Gugino *et al.*, 2001; John, 2002; Purdon *et al.*, 2013). On the contrary, animal studies suggest that transitions into and out of anaesthesia-induced unconsciousness may be governed by different mechanisms (Kelz *et al.*, 2008; Shirasaka *et al.*, 2011). Moreover, an exposure to the general anaesthetic propofol has been suggested to induce long-lasting impairment in neurons (Kline *et al.*, 2012; Krzisch *et al.*, 2013). Neurophysiological recovery from anaesthesia can be affected by neuronal damage that may be taking place during anaesthetic exposure. Here, we have developed a non-human primate model to investigate neurophysiological recovery following propofol anaesthesia by directly recording from a functionally and anatomically interconnected somatosensory (S1 and S2) and ventral premotor area (PMv) network (Kurata, 1991; Tanne-Gariepy *et al.*, 2002; de Lafuente and Romo, 2006; Garbarini *et al.*, 2019). The PMv is known to link sensation and decision-making as well as to integrate multisensory modalities (Rizzolatti *et al.*, 2002; de Lafuente and Romo, 2005, 2006; Pardo-Vazquez *et al.*, 2008; Lemus *et al.*, 2009; Acuna *et al.*, 2010; Romo and de Lafuente, 2013).

Materials and methods

We used two adult male monkeys (*Macaca mulatta*, 10–12 kg). All animals were handled according to the institutional standards of the National Institutes of Health and according to an animal protocol approved by the institutional animal care and use committee. Prior to starting the study, a titanium head post and a vascular access port in the internal jugular vein were surgically implanted in each animal. The extracellular microelectrode arrays (Floating Microelectrode Arrays, MicroProbes) were implanted into the primary somatosensory cortex (S1), the secondary somatosensory cortex (S2) and ventral premotor area (PMv) through a craniotomy (Fig. 1A). The animals were trained in a behavioural task (Fig. 1B) in which their trial-by-trial alertness was determined by a push-button response. The animal was required to initiate a trial by pressing a button within 1.5 s after the start tone and keep its hand on the button until the end of the trial in order to receive a liquid reward (correct response). Failed attempts included late button press and early hand release. Independent tactile (air puff) and sound stimuli were delivered alone or in combination during each trial to examine multisensory responses in this network. The animal's performance during the session was monitored and simultaneously recorded using a MATLAB-based behaviour control system, MonkeyLogic (Asaad and Eskandar, 2008) (Fig. 1C). We defined two metrics to allow quantification of behavioural end points: task engagement and task performance probability. Task engagement indicates a probability of any response initiation, including correct responses and failed attempts, and task performance represents a probability of correct responses only (Wong *et al.*, 2011, 2014) (Fig. 1C).

A general anaesthetic (propofol) was infused for 60 min at a fixed rate (200 μg/kg/min for Monkey 1 and 230 or 270 μg/kg/min for Monkey 2) through a vascular access port following 30 min of awake performance (Fig. 1C). No other sedatives or anaesthetics were used during the experiment. The animal's heart rate and oxygen saturation were continuously monitored throughout the session (CANL-425SV-A Pulse Oximeter, Med Associates). The animals maintained >94% of oxygen saturation throughout the experiments.

Neural activity was recorded continuously and simultaneously from S1, S2, and PMv through the microelectrode arrays throughout anaesthesia and recovery. Analogue data were amplified, band-pass filtered between 0.5 Hz and 8 kHz and sampled at 40 kHz (OmniPlex, Plexon). Local field potentials (LFPs) were separated by low-pass filtering at 200 Hz and down-sampled at 1 kHz. The spiking activity was obtained by high-pass filtering at 300 Hz, and a minimum threshold of 3 standard deviations (SDs) was applied to exclude background noise from the raw voltage tracings on each channel. Action potentials were sorted using waveform principal component analysis (Offline Sorter, Plexon). All LFP and single-unit analyses were performed using existing and custom-written functions in MATLAB (MathWorks Corp). Multitaper spectral analysis of the LFP, using the Chronux toolbox for MATLAB, was used to generate spectra, spectrograms, and power changes over time. Five-second time windows were used when generating spectrograms or calculating power changes in a particular band over time. Peak frequency calculation was performed by first finding the frequency at which spectral power was maximum within the beta range (14–30 Hz) for each behavioural end point; awake, ROC and return of pre-anaesthetic performance (ROPAP) and pooling the data from each session. One-way Kruskal-Wallis with *post hoc* Dunn's tests were used for the peak frequencies between the three behavioural groups. Time-varying changes in coherence were calculated at each frequency over 10-s time bins. These data were then used to generate coherence time-frequency plots and line coherograms. Peak frequency within the beta range (14–30 Hz) was calculated for coherence at awake (before anaesthesia start), immediately following ROC and immediately following ROPAP for a 1-min window. Event-aligned time-varying changes in coherence were calculated with a 0.5-s sliding window and 20% overlap, restricted to 4 s around the event of choice per trial. These data were then

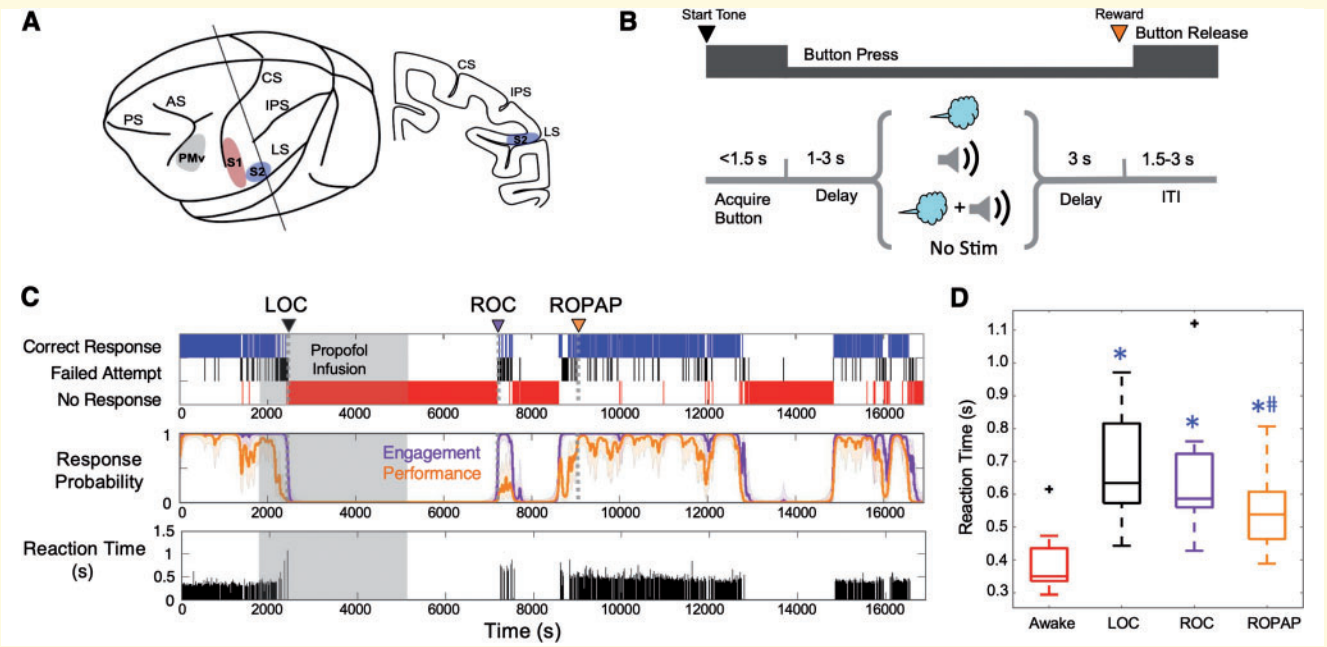

Figure 1 Experimental paradigm and behavioural responses. (**A**) Location of the recording sites. Neural recording is performed in the primary somatosensory cortex (S1, red), secondary somatosensory cortex (S2, blue) and ventral premotor cortex (PMv, grey). AS = acuate sulcus; CS = central sulcus; IPS = intraparietal sulcus; LS = lateral sulcus; PS = principal sulcus. (**B**) Behavioural task (multisensory task). Sequence of events during behavioural trials. At the start tone (pure tone 1000 Hz 100 ms) the animal initiates a trial by placing the hand (ipsilateral to the recording site) on the button in front of the animal. After a random delay, one of the four different sensory stimulus sets is presented for 250 ms. The animal is required to keep its hand on the button until the end of the trial in order to receive a liquid reward (correct response). The animal then has to release the button during the intertrial interval (ITI). One of the four stimulus sets (air puff, sound, simultaneous air puff and sound, or no stimulus) was randomly delivered to the animals in every trial regardless of their button response. Air puff was delivered at 12 psi to the lower face and a pure tone of 4000 Hz was delivered at 80 dB SPL (both for 250 ms). (**C**) Typical behavioural response during propofol anaesthesia and recovery. *Top*: The animal's trial-by-trial button response. Correct responses (blue), failed attempts (black), and no response (red). *Middle*: Probability of the task engagement (purple) and task performance (orange). *Bottom*: The trial-by-trial reaction time (from start tone to button press). (**D**) Reaction times. Box plots for the reaction time over 30 trials during wakefulness (Awake), immediately prior to loss of consciousness (LOC), at return of consciousness (ROC), and at return of pre-anaesthetic performance (ROPAP). Outliers are shown with a black cross. There is a significant effect of anaesthetic-induced altered states of consciousness (awake, LOC, ROC, and ROPAP) on the reaction time [ANOVA $F(3,59) = 25.6$, $P = 2.1 \times 10^{-8}$]. An asterisk indicates a significant difference from the awake state (*post hoc* Turkey-Kramer test, $P < 0.01$). A hash symbol indicates a significant difference from LOC ($P = 0.024$). LOC is shown with a black arrow and dotted lines, ROC with a purple arrow and dotted lines, and ROPAP with an orange arrow and dotted lines (**C**). Propofol was infused at 200 μg/kg/min from 1800 to 5400 s (shaded area in **C**).

averaged across a maximum of 100 trials and used to generate coherence time-frequency plots.

To characterize the anaesthesia-induced brain states and their transitions, a 2D state space was defined using two spectral amplitude ratios as reported by Gervasoni *et al.* (2004). Briefly, we obtained two frequency-band spectral power ratios (Ratio 1 = $power_{16\text{-}30\,Hz}/power_{0.5\text{-}60\,Hz}$ and Ratio 2 = $power_{0.5\text{-}6\,Hz}/power_{0.5\text{-}15\,Hz}$) as the absolute value under the curve of each calculation from each channel. For each region and ratio, all data were concatenated in a time-by-channel matrix and subjected to principal component analysis. The first principal component (PC1) explained >70% of the data, on both ratios. We smoothed the PC1 values by running a 20-s Hanning window to reduce instant variability. All figures are cloud representations of both ratios' PC1s single values, where each point represents 1 s of time, and coloured with different heat maps. The data density was calculated with a kernel density estimator function. The speed was calculated as the Euclidean length between consecutive points. The trajectory-speed plots show the speed values only for 20 min of data around the LOC and ROC. The engagement plots represent the same values calculated above. Additionally, to quantify the rate of change in oscillatory power in the spectrograms, we computed the first derivative within each frequency band of interest immediately around ROC. We computed the peak of the first derivative in each band accounting for both positive and negative rates of change (e.g. power increasing or decreasing relative to ROC) across sessions. We then performed a Kruskal-Wallis non-parametric test on the positive and negative peaks of the first derivative across each frequency-band of interest. *Post hoc* analyses were performed with a Tukey-Kramer test.

Sensory responsive neurons were categorized into four groups based on their response to a puff or sound stimulus during wakefulness: bimodal puff and sound responsive neurons with enhanced firing response; bimodal puff and sound responsive neurons with suppressed firing response; unimodal puff responsive neurons; or unimodal sound responsive

neurons. Peri-stimulus time histograms were constructed for each neuron by binning spiking data into 1-ms bins and convolving a Gaussian function (SD = 50 ms) during a 4-s time window centred on the stimulus delivery.

The predicted propofol concentration was calculated based on a three compartment pharmacokinetic (PK) model using the parameters reported by Miyabe-Nishiwaki *et al.* (2010, 2013). The total simulation time was 300 min, with a time resolution of 0.25 s. The drug dosage was adjusted to each animal's experimental infusion rate, starting at 30 min and ending at 90 min. Predicted propofol concentrations in each compartment were calculated at LOC, ROC, and ROPAP, based on each animal's behavioural response.

Data availability

The data that support the findings of this study are available from the corresponding author, upon reasonable request.

Results

Recovery end points can be determined by task engagement and performance

We have successfully determined probability of the animal's task engagement and task performance by their button response throughout anaesthesia and recovery (Fig. 1C). We then evaluated how the ROC time is affected by varying the probability threshold for task engagement (Supplementary Fig. 1A). For the vast majority of sessions, task engagement increased swiftly from probability thresholds of 0.2 to 0.8 within three to seven trials. For a small subset of the sessions, however, ROC times appeared to be affected by varying the probability threshold, especially between 0.2 and 0.5. We chose an engagement threshold of 0.3 as an approximate 50% point of the ROC time change. This threshold allowed earlier detection of the initial moment of recovery. For all subsequent analyses, ROC was defined as the first time, since being unconscious, at which the probability of task engagement was >0.3 (Fig. 1C). Additionally, we defined ROPAP as the behavioural end point to indicate recovery of performance to a level equivalent to pre-anaesthetic performance. ROPAP was defined as the first time, since being unconscious, at which the probability of a correct response was >0.9 (Fig. 1C). Additionally, we examined speed of the task responses during anaesthesia and recovery to further characterize the recovery end points (Fig. 1C). The reaction time (from start tone to button press) significantly changed by anaesthetic-induced altered states of consciousness [awake, LOC, ROC, and ROPAP, ANOVA $F(3,46) = 25.6$, $P = 6.8 \times 10^{-10}$] (Fig. 1D). Reaction time during wakefulness was significantly shorter than any of the following behavioural points (*post hoc* Tukey-Kramer test, $P < 0.001$). However, there was no statistically significant difference between the reaction time at LOC and ROC ($P = 0.112$).

Spatiotemporally distinct neuronal dynamics are associated with return of consciousness

We first compared LFP spectrograms from each of the cortical areas during the transition from propofol-induced unconsciousness to consciousness. We found that ROC coincided with a distinctive return of beta oscillations in both S1 and PMv and a concurrent decline of slow-delta oscillations that were dominant during unconsciousness (Fig. 2A–E). Prior, during the period between the end of propofol infusion and ROC, we found a transient increase in the slow-delta power in S1 and S2 while slow-delta power decreased in PMv [Fig. 2H(i)]. On the contrary, theta, alpha and low beta power increased in PMv upon the end of propofol infusion, but remained at the same level in S1 and S2 [Fig. 2H(ii–iv)], together suggesting that regional dynamics are dissociated between S1 and PMv in a frequency-specific manner during an early transitional period to ROC. ROPAP was observed during an increase in beta power and was not associated with distinct neural changes (Fig. 2A–E). Peak frequency of the characteristic beta oscillations appeared to be increasing from ROC to ROPAP, but remained statistically significantly lower at ROPAP than that during wakefulness (Fig. 2F and G).

Focusing on the state transitions, we then investigated clusters in the 2D state space and velocity of their transitions (Gervasoni *et al.*, 2004; Hudson *et al.*, 2014). We found two distinct clusters shown by two high density cores in both S1 and PMv (Fig. 3A). These two high density clusters were connected by regions of low densities. These connecting areas corresponded to high speed values of spontaneous trajectories (Fig. 3B), indicating rapid or unstable transitions. We further examined the speed changes around the time of LOC and ROC (Fig. 3C and D). ROC was found during a rapid transition in S1 and PMv while the transition around LOC appeared to be slower than ROC. Moreover, these clusters were clearly distinguished by the animal's task engagement level (Fig. 3E), especially one of the clusters was exclusively associated with zero or minimum task engagement (Fig. 3E). We further quantified the rate of spectrographic change (Fig. 3F–I). The first derivative within each frequency band is shown immediately before and after ROC in Fig. 3F and G. We found significant changes in peak of the first derivative in both S1 [Kruskal Wallis Test, $\chi^2(5) = 24.7$, $P = 1.58 \times 10^{-4}$] and PMv [$\chi^2(5) = 28.2$, $P = 3.29 \times 10^{-5}$] and observed significant differences between lower frequency bands (slow delta and theta)

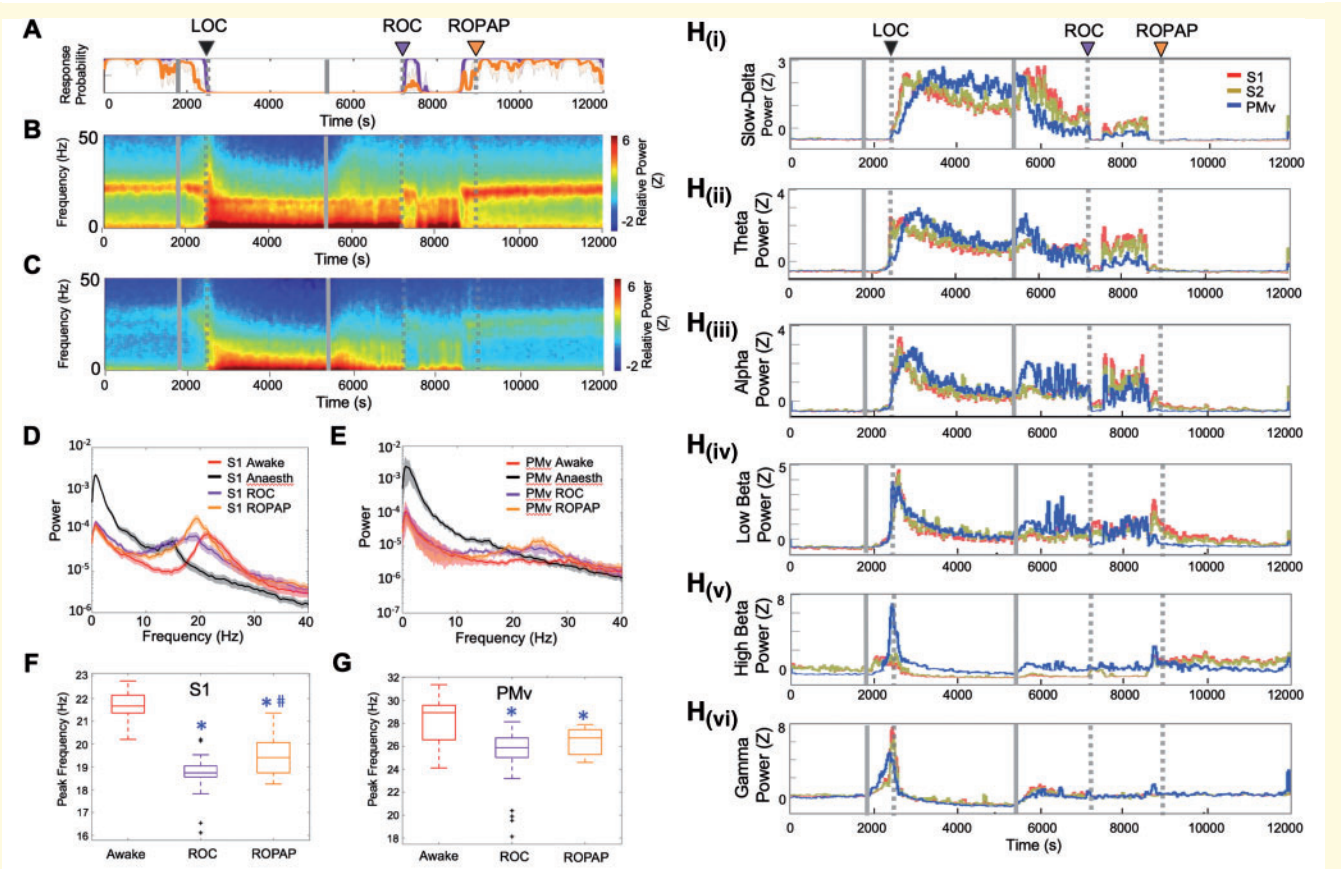

Figure 2 Return of the beta oscillations and decline of the slow-delta oscillations are associated with ROC. (**A**) Behavioural response. (**B**) LFP spectrograms in S1. (**C**) LFP spectrograms in PMv. (**D**) Power spectrum in S1. (**E**) Power spectrum in PMv. The spectra are shown during wakefulness (Awake), anaesthesia (the last 15 min of propofol infusion), ROC and ROPAP. (**F**) Peak frequencies of the beta oscillations in S1; 21.7 ± 0.1 Hz in awake, 18.8 ± 0.1 Hz at ROC, 19.4 ± 0.1 Hz at ROPAP (mean ± SE). An asterisk indicates a significant difference from the awake state [one-way Kruskal-Wallis for S1: $\chi^2(2) = 220.0$, $P = 1.68 \times 10^{-48}$, *post hoc* Dunn-Sidak test, $P < 0.001$]. A hash symbol indicates a significant difference from ROC ($P = 0.015$). Outliers are shown with a black cross. (**G**) Peak frequencies in PMv; 28.0 ± 0.2 Hz in awake, 25.4 ± 0.3 Hz at ROC, 26.4 ± 0.1 Hz at ROPAP (mean ± SE). An asterisk indicates a significant difference from the awake state [one-way Kruskal-Wallis for PMv: $\chi^2(2) = 50.06$, $P = 1.35 \times 10^{-11}$, *post hoc* Dunn-Sidak test, $P < 0.001$]. Outliers are shown with a black cross. (**H**) Change of the power in slow-delta [0.5–4 Hz, **H(i)**], theta [4–8 Hz, **H(ii)**], alpha [8–12 Hz, **H(iii)**], low beta [12–18 Hz, **H(iv)**], high beta [18–25 Hz, **H(v)**], low gamma [25–34 Hz, **H(vi)**] for S1 (red), S2 (brown) versus PMv (blue). Power was normalized using z-scores. Propofol was infused for 60 min (1800–5400 s, grey solid lines in **A**–**C**, and **H**). LOC is shown with a black arrow and dotted lines, ROC with a purple arrow and dotted lines, and ROPAP with an orange arrow and dotted lines (**A**–**C**, and **H**).

versus high frequency bands (low beta, high beta and low gamma) (Fig. 3H and I).

We next investigated how communication between these regions changed during ROC by examining both local and regional coherence changes. We found that the beta oscillations were immediately coherent locally and interregionally when they returned at ROC (Fig. 4A–C). Interestingly, we reported that, prior to LOC, the interregionally coherent beta oscillations were disrupted while the animals were still engaged in the task (Ishizawa *et al.*, 2016), together suggesting different interregional dynamics between LOC and ROC. Upon task performance recovery (ROPAP), interregional coherence significantly increased in power compared to ROC (Fig. 4B–E), but the peak frequency of the coherent beta oscillations was still significantly lower than that during wakefulness (Fig. 4F and G). Moreover, we focused on how interregional coherence was organized around task events in each trial. When the animal was awake and performing, the beta-range coherence appeared to be dominant during the pre-trial period (before start tone) and beta coherence was briefly disrupted upon the button press (Fig. 4H). There is a brief increase of coherence in the low frequencies at the time of puff and sound stimulation, likely corresponding to evoked responses to puff and sound. These results suggest that the regions are functionally connected. During propofol anaesthesia, there is a wide-band increase in coherence at the time of puff stimulation, but there were no other task event-related changes. The event-related coherence was reorganized after ROPAP with the exception of its response to sound stimulation.

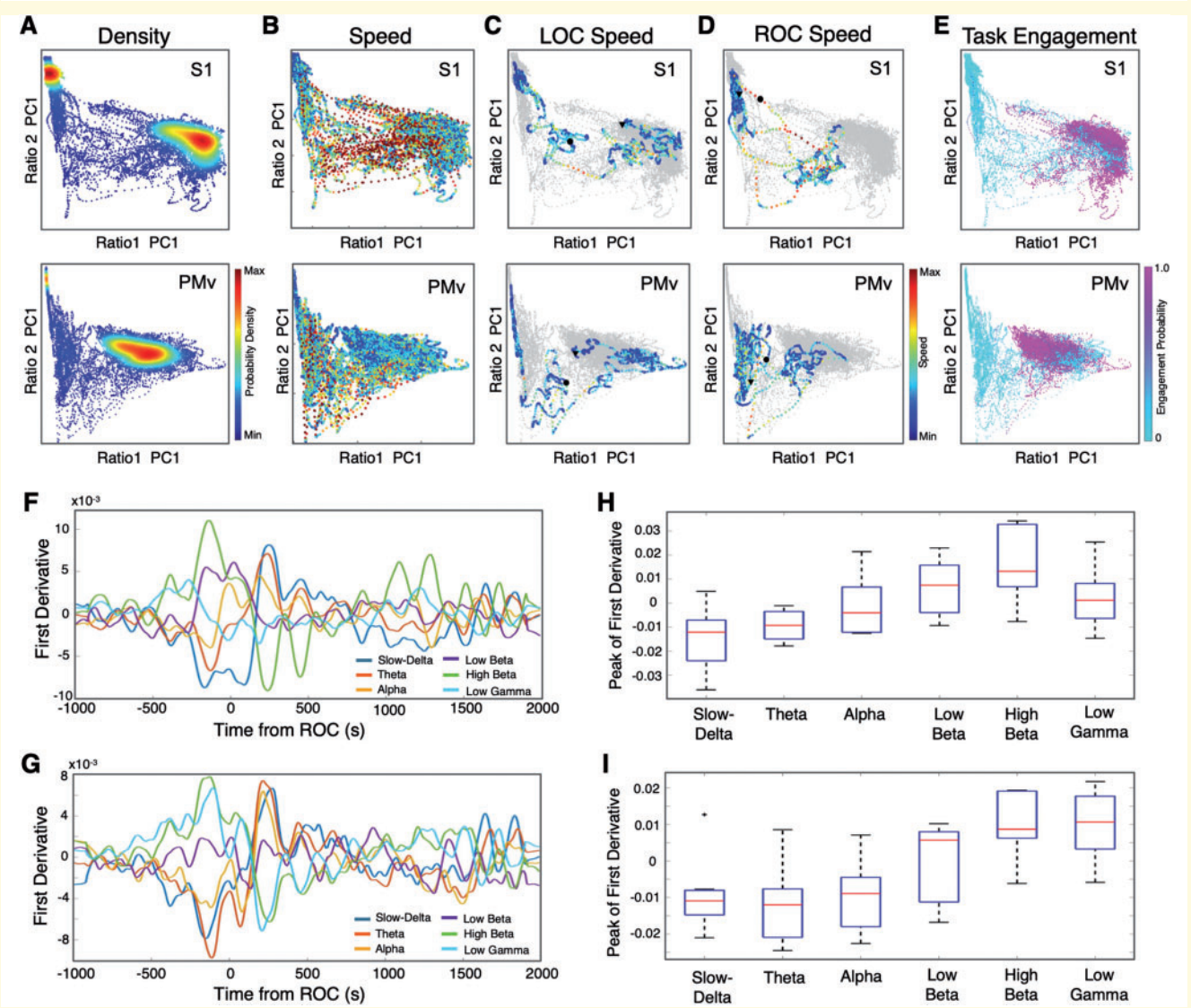

Figure 3 Clusters in 2D state space correspond to distinct behavioural states and the state transitions are rapid. (**A**) Density plots. The density was calculated from the scatter plots that were created using two chosen LFP spectral amplitude ratios. Each dot corresponds to a 1-s window for which the amplitude ratios were calculated through the course of wakefulness, anaesthesia and recovery (one recording session of 4.5 h is displayed). (**B**) Speed plots. The plots represent the average velocity of spontaneous trajectories within the 2D state space. (**C**) Speed plots during LOC. The plots are shown for the 20-min period around LOC (10 min before and 10 min after LOC). A black circle indicates the time of LOC and a triangle indicates the start dot of the 20 min. (**D**) Speed plots during ROC. The plots are shown for the 20 min around ROC (10 min before and 10 min after ROC). A black circle indicates the time of ROC and a triangle indicates the start point of the 20 min. (**E**) Task engagement. The plots are colour coded according to the task engagement probability. Each cluster corresponds to a distinct state, high engagement, or low or no engagement. (**F** and **G**) First derivatives for each frequency band. The first derivatives (dy/dx) were computed for the average power within each frequency band centred on ROC (1000 s before and 2000 s after) for S1 (**F**) and PMv (**G**): slow-delta (0.5–4 Hz), theta (4–8 Hz), alpha (8–12 Hz), low beta (12–18 Hz), high beta (18–25 Hz), and low gamma (25–34 Hz). (**H** and **I**) Peak of the first derivatives. The peak of the first derivatives, either positive or negative, were computed to indicate the maximum rate of change within each frequency band of interest in a window immediately preceding ROC for S1 [Kruskal-Wallis $\chi^2(5) = 24.7$, $P = 1.58 \times 10^{-4}$; **H**] and PMv [Kruskal-Wallis $\chi^2(5) = 28.2$, $P = 3.29 \times 10–^{5}$; **I**]. In S1, peak of low beta is significantly higher than slow-delta (*post hoc* Tukey-Kramer test, $P < 0.018$; **H**). Peak of high beta is significantly higher than slow-delta ($P = 0.0006$; **H**) and theta ($P = 0.0045$; **H**). In PMv, peak of both high beta and low gamma are significantly higher than slow-delta, theta, and alpha in PMv (*post hoc* Tukey-Kramer test, all $P < 0.02$; **I**).

The sequence of neuronal dynamics observed during recovery was also identified in the animals that were not performing the task (Supplementary Fig. 2) and in the blindfolded animals that were performing the task (Supplementary Fig. 3). These results suggest that the observed neuronal dynamics were not the consequences of the return of their task response or eye opening. Interestingly, we have observed a period of oscillatory

dynamics change without a corresponding behavioural response prior to ROC in a blindfolded animal (Supplementary Fig. 3). A similar change was observed in the other blindfolded session. These results suggest that in certain conditions, such as blindfolding, there could be a delay in the task response return despite the spectrographic change that suggests ROC. We did not observe ROC without a concurrent change in neural dynamics. Moreover, in alert task-performing animals, return of task response after arbitrary breaks was not associated with concurrent neuronal dynamics changes (Ishizawa *et al.*, 2016), suggesting that return of motivation *per se* is unlikely associated with observed neural changes.

We also tested arousability in two separate recording sessions in one animal. We applied a series of stimuli [non-aversive ear-pulling, a loud white noise at 100 dB SPL (sound pressure level) for 5 s, and three hand claps at 10 cm from the face] at 3 min, 10 min, and 30 min from the LOC, at the end of anaesthetic infusion, and at 10 min after the end of infusion. We did not observe return of a task attempt at any of these time points in the animal.

Region-specific cortical spiking activity during return of consciousness

We next investigated single neuron responses during recovery from propofol-induced unconsciousness. We recorded 640 well-isolated single neurons, including 477 neurons (in S1, S2, and PMv) in Monkey 1 during 18 experimental sessions and 163 neurons (in S1 and PMv) in Monkey 2 during 11 sessions, of which 331 (51.7%) were sensory-responsive to either tactile or auditory stimulation ($n = 193$ in S1; $n = 58$ in S2; $n = 80$ in PMv) (Ishizawa *et al.*, 2016). The average firing rate significantly decreased during propofol anaesthesia and started increasing upon the end of propofol infusion (Fig. 5A). Recovery of firing rates in the PMv neurons appeared to precede S1 and S2 neurons following the end of anaesthesia. Interestingly, firing rates decreased in PMv upon ROC while the firing rates continued to increase in S1 and S2. These regional differences in spike firing rates were not observed at the return of their task response during wakefulness (Ishizawa *et al.*, 2016). A recent study has shown a population of neurons in the medial prefrontal cortex that significantly increase their firing rates during periods of inattention and eye closure (Gabbott and Rolls, 2013), together suggesting region-specific firing response during altered states of alertness.

Multisensory response recovery is associated with performance recovery

Lastly, we focused on the recovery of sensory processing in these cortical neurons. We first identified distinct subpopulations of neurons on the basis of their responsiveness to the sensory stimulation during wakefulness. S2 neurons were recorded from only one monkey and we focused our analyses on S1 and PMv neurons. We then excluded neurons from recording sessions in which ROPAP was detected within 100 trials from ROC ($n = 84$ in S1, $n = 39$ in PMv) to characterize the sensory response possibly associated with ROC and ROPAP. Statistically significant puff responses remained during propofol anaesthesia while sound responses appeared to be almost completely diminished (Fig. 5B and C) (Ishizawa *et al.*, 2016). The unimodally puff-responsive S1 and PMv neurons appeared to recover through ROC and return to the awake level at the time around ROPAP (Fig. 5B and C). Bimodal puff and sound responsive neurons also appeared to recover their response at ROPAP. The sound response in S1 bimodal neurons did not reach pre-anaesthetic levels at ROPAP. Further, we analysed peri-stimulus time histograms at the average ROC time [36 ± 7 min after the end of propofol infusion, mean ± standard error (SE)] and the average ROPAP time (109 ± 8 min after the end of propofol infusion, mean ± SE) across sessions (Supplementary Fig. 4A and B) to demonstrate temporal recovery of sensory responses as compared to the recovery associated with session-specific behavioural end points. In bimodally responsive S1 and PMv neurons, including enhanced and suppressed responses, all sound responses were still significantly smaller at the average ROPAP time compared with those during wakefulness (Kruskal-Wallis Test, $P < 0.01$), suggesting that the recovery of multisensory responses in these neurons is associated with performance recovery rather than the length of recovery time.

Discussion

Our results demonstrate that ROC from general anaesthesia corresponds with an abrupt shift of neuronal dynamics across the primate neocortex, even though pharmacokinetics assures a gradual decline of the brain anaesthetic concentration. We found that the ROC, defined as return of task engagement, was marked with an abrupt shift to regionally coherent beta oscillations and disruption of the slow-delta oscillations in a somatosensory and premotor network. Prior to ROC, following the end of the anaesthetic infusion, oscillatory dynamics in these cortical regions appeared to be dissociated. Together with the dynamics during propofol-induced LOC (Ishizawa *et al.*, 2016), transitional periods of LOC and ROC are both characterized by: (i) distinctive, not gradual, neural changes; (ii) involving a period of interregional dissociation; and (iii) being imposed between two apparently stable coherent states, such as wakefulness and unconsciousness. Discrete metastable states have been shown during emergence from isoflurane in small animals (Hudson *et al.*, 2014). Abrupt state transitions are well known during natural sleep (Gervasoni *et al.*, 2004). We also demonstrate rapid transitions between two distinct

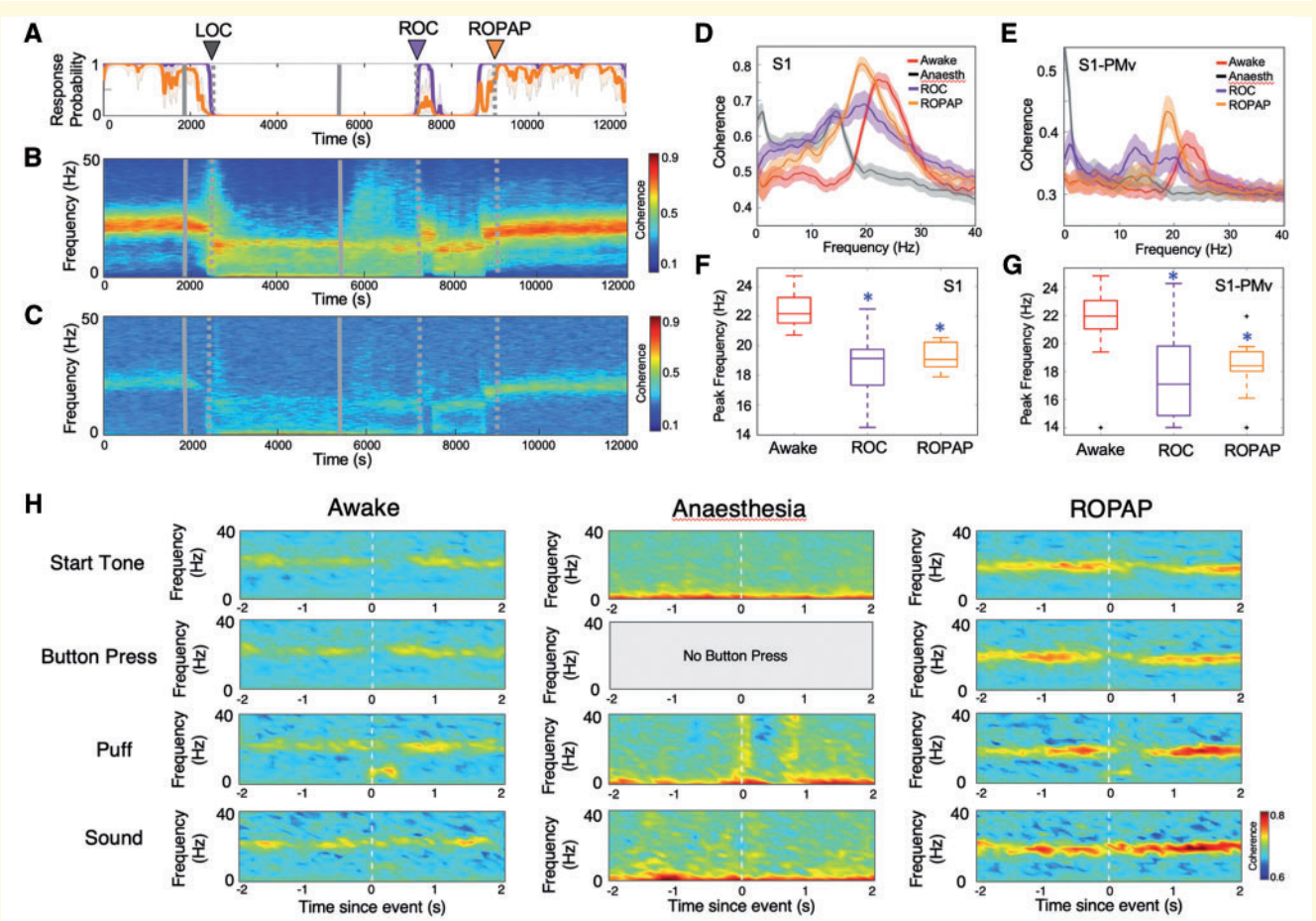

Figure 4 Beta oscillations are interregionally coherent at ROC and the coherence further increases at ROPAP. (**A**) Behavioural response. (**B**) LFP coherence time-frequency plot in S1. (**C**) LFP coherence time-frequency plot between S1 and PMv. (**D**) Coherence within S1 at awake (before anaesthesia start, red trace), anaesthesia (before the end of anaesthesia infusion, black trace), immediately following ROC (purple trace) versus immediately following ROPAP (orange trace). Coherence was averaged for a 1-min period for each epoch. Lines are shown with shaded standard error bands. (**E**) Coherence between S1 and PMv at awake (before anaesthesia start, red trace), anaesthesia (before the end of anaesthesia infusion, black trace), immediately following ROC (purple trace) versus immediately following ROPAP (orange trace). Coherence was averaged for a 1-min period for each epoch. Lines are shown with shaded standard error bands. (**F**) Peak beta frequencies of the coherence within S1 at awake (before anaesthesia start, red trace), immediately following ROC (purple trace) versus immediately following ROPAP (orange trace) for 1 min. There is a significant effect of anaesthetic-induced altered states of consciousness (awake, ROC, and ROPAP) on the peak frequency [ANOVA $F(2,42) = 22.8$, $P = 2.0 \times 10^{-7}$]. An asterisk indicates a significant difference from the awake state (*post hoc* Turkey-Kramer test, $P < 0.0001$). (**G**) Peak beta frequencies of the coherence between S1 and PMv at awake (before anaesthesia start, red trace), immediately following ROC (purple trace) versus immediately following ROPAP (orange trace) for 1 min. There is a significant effect of anaesthetic-induced altered states of consciousness (awake, ROC, and ROPAP) on the peak frequency [ANOVA $F(2,42) = 11.8$, $P = 8.8 \times 10^{-5}$]. An asterisk indicates a significant difference from the awake state (*post hoc* Turkey-Kramer test, $P < 0.005$). Outliers are shown with a black cross. (**H**) Task-event related change in the coherence between S1 and PMv. The time frequency coherence plots are the average across trials for start tone ($n = 100$ trials), button press ($n = 100$ trials), puff stimulation ($n = 49$ trials) and sound stimulation ($n = 37$ trials). Each column represents different time epochs; immediately before anaesthesia start (Awake), immediately before anaesthesia end (Anaesthesia), and immediately following ROPAP. Propofol was infused for 60 min (1800–5400 s, grey solid lines in **A**–**C**). LOC is shown with a black arrow and dotted lines, ROC with a purple arrow and dotted lines, and ROPAP with an orange arrow and dotted lines in **A**–**C**.

stable clusters corresponding to anaesthesia and wakefulness (Fig. 3). These results together suggest that abrupt state transitions are a fundamental manner of how the brain functions. It is possible that the observed regional dissociation may reflect destabilization of the network which eventually results in an abrupt transition to consciousness (Hudson *et al.*, 2014).

Despite structural similarities between LOC and ROC, actual oscillatory dynamics are unique to LOC and ROC in these regions and are not simply inverses of each other. We reported locally-coherent, but not interregionally coherent, prominent beta-gamma peak corresponding to LOC in this cortical network (Fig. 2F) (Ishizawa *et al.*, 2016). The high frequency peak was not observed

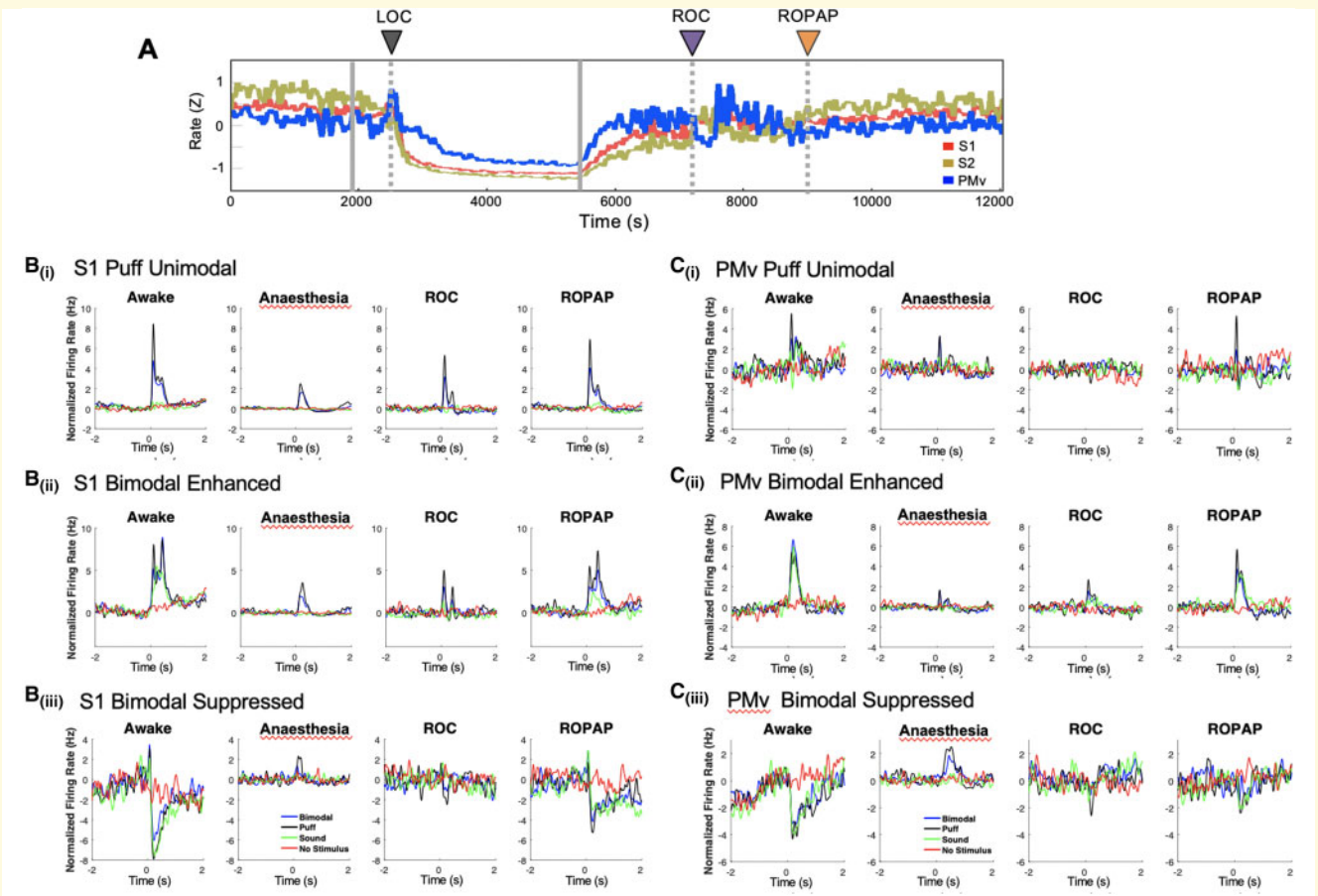

Figure 5 Neuronal firing rate and multisensory responses in S1 and PMv. (**A**) Average baseline firing rates in S1, S2 and PMv. Firing rates were normalized using z-scores. (**B**) Peri-stimulus time histograms for S1 unimodal tactile-responsive neurons [**B(i)**], bimodal tactile and auditory responsive neurons [**B(ii)**], and bimodal neurons with suppressed firing rate response [**B(iii)**] during wakefulness, anaesthesia, ROC and ROPAP. (**C**) Peri-stimulus time histograms for PMv unimodal tactile-responsive neurons [**C(i)**]. Bimodal tactile and auditory responsive neurons [**C(ii)**], and bimodal neurons with suppressed firing rate response [**C(iii)**] during wakefulness, anaesthesia, ROC and ROPAP. LOC is shown with a black arrow and dotted lines, ROC with a purple arrow and dotted lines, and ROPAP with an orange arrow and dotted lines in **A**.

during ROC. Although interregional beta coherence was disrupted prior to LOC while the animals were still engaged in the task, the interregional coherence was returned at the time of the return of task engagement (ROC) during recovery. These results suggest that LOC and ROC may be governed by different neural processes. Moreover, we successfully determined ROPAP as an end point of full task performance recovery. ROPAP was identified during a gradual increase of the characteristic beta oscillations in power. The peak beta frequencies at ROPAP, however, were still lower than the awake level, suggesting that full task performance recovery may not require full recovery of oscillatory dynamics. Interestingly, we found that speed of task response was still significantly lower at ROPAP than that during wakefulness (Fig. 1D), which might be attributed to nearing but not complete recovery of the dynamics. In addition, our results suggest that recovery of single neuron responses, especially multisensory processing, appear to correlate with the performance recovery, but not simply with the duration of the recovery time.

We also found that recovery end points significantly varied intra-individually across sessions, as compared to a rather consistent LOC time. For instance, the ROC time (since the end of anaesthetic infusion) varied from 11 min to 122 min in Monkey 1, and 16 min to 65 min in Monkey 2. Similarly, the ROPAP time varied. With no apparent changes in the pharmacokinetic variables across sessions in each animal, a critically lowered anaesthetic concentration *per se* is unlikely to lead to ROC. We further studied predicted propofol concentrations in each animal to examine how the predicted propofol concentrations change around the time of LOC and ROC. We applied a three-compartment pharmacokinetic (PK) model using the parameters reported in Japanese macaque monkeys (*M. fuscata*) (Miyabe-Nishiwaki *et al.*, 2010, 2013) (Fig. 6A

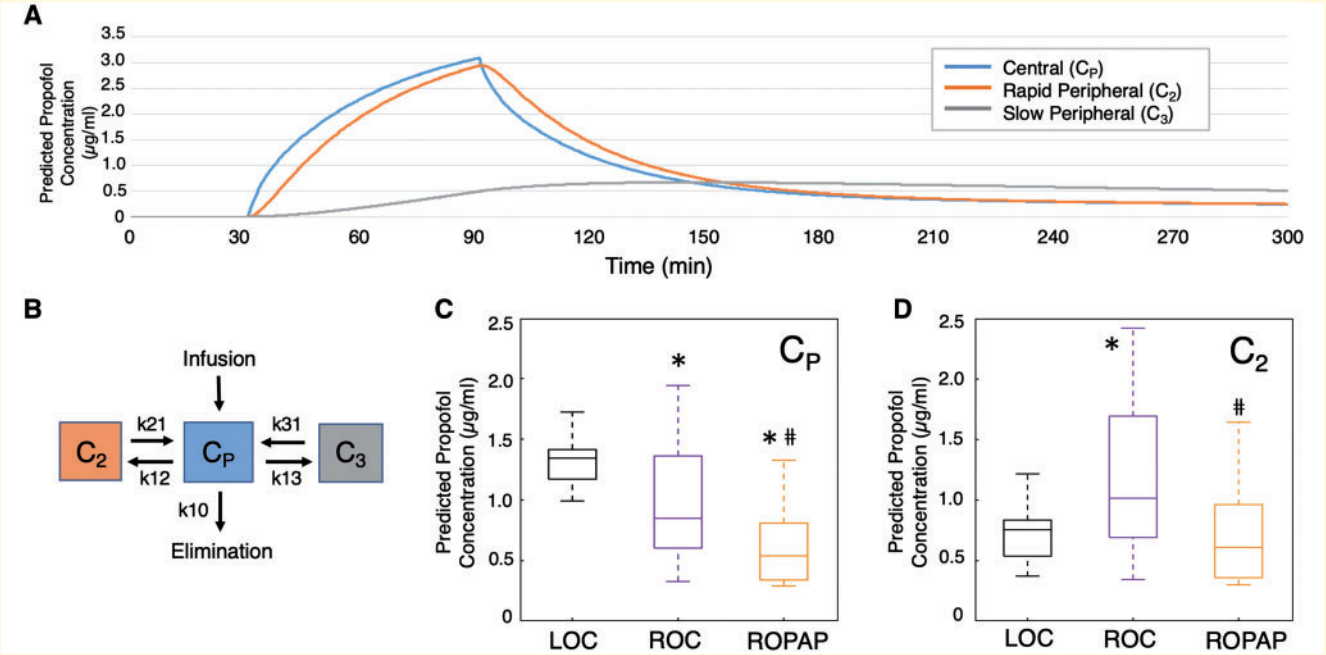

Figure 6 Pharmacokinetic predictions of propofol concentrations. (**A**) Predicted propofol concentrations during anaesthesia and recovery. (**B**) Three-compartment pharmacokinetic (PK) model. Propofol concentrations in each compartment were calculated using the parameters reported in Japanese macaque monkeys. The parameter estimates of clearance and distribution volume are 9.05 l/min and 0.36 l/min, respectively, for central compartment (Cp), 8.29 l/min and 1.16 l/min for rapid peripheral compartment (C2), and 68.3 l/min and 0.293 l/min for slow peripheral compartment (C3) (Miyabe-Nishiwaki *et al.*, 2010, 2013). Kinetic values are shown k = clearance (CL)/distribution volume (V). k10 = CLp/Vp; k12 = CL2/Vp; k21 = CL2/V2; k13 = CL3/Vp; k31 = CL3/V3. (**C**) Predicted propofol plasma concentrations (Cp) at LOC, ROC, and ROPAP. An asterisk indicates a significantly lower concentration than LOC at ROC (two-sided Wilcoxon rank sum tests, $P = 0.006$) and at ROPAP ($P = 1.9 \times 10^{-7}$). A hash symbol indicates a significantly lower concentration than ROC at ROPAP ($P = 0.002$). (**D**) Predicted propofol concentration in rapid peripheral compartment (C_2) at LOC, ROC, and ROPAP. *Significantly higher concentration than LOC at ROC (two-sided Wilcoxon rank sum tests, $P = 0.018$). #Significantly lower concentration than ROC at ROPAP ($P = 0.002$).

and B). The PK model indicated that predicted propofol plasma concentrations (Cp) at LOC and ROC were 1.32 ± 0.17 μg/ml and 0.97 ± 0.46 μg/ml (two-sided Wilcoxon rank sum tests, $P = 0.006$), respectively, suggesting discrepancy or hysteresis between LOC and ROC (Sepulveda *et al.*, 2018) (Fig. 6C). However, interestingly, predicted propofol concentration in rapid peripheral compartment (C_2) at ROC was higher than the one at LOC (1.17 ± 0.60 μg/ml at ROC versus 0.71 ± 0.19 μg/ml at LOC, $P = 0.018$) (Fig. 6D). In addition, large variability was found for both Cp and C_2 at ROC compared to rather a narrow distribution of Cp and C_2 at LOC (Fig. 6C and D). These results suggest that the behavioural recovery is independent from the anaesthetic pharmacokinetics. The results are also consistent with the recently proposed stochastic model that indicates collapse of hysteresis and variability of recovery time by Proekt and Hudson (2018). Nevertheless, our results demonstrate that transitions of anaesthetic-induced unconsciousness and consciousness are accompanied by discrete changes in the cortical dynamics, and the state transitions may not be directly prompted by the anaesthetic pharmacokinetics. Investigating how the brain dynamics in a broader network plays a role in these state transitions will further elucidate the mechanisms of recovery from general anaesthesia.

Acknowledgements

We thank Tatsuo Kawai, MD for performing vascular port surgeries in primates, Anne Smith, PhD for expert assistance in the behavioural analyses, Sourish Chakravarty, PhD for expert assistance in the pharmacokinetic model analyses, and Warren M. Zapol, MD for guiding and supporting the project development.

Funding

This work was supported by grants from the Foundation for Anesthesia Education and Research, the National Institute of Health (5T32GM007592, 1P01GM118269), and Harvard Medical School (Eleanor and Miles Shore 50th Anniversary Fellowship Scholars in Medicine).

Competing interests

The authors report no competing interests.

Supplementary material

Supplementary material is available at *Brain* online.

References

Acuna C, Pardo-Vazquez JL, Leboran V. Decision-making, behavioral supervision and learning: an executive role for the ventral premotor cortex? Neurotox Res 2010; 18: 416–27.

Asaad WF, Eskandar EN. A flexible software tool for temporally-precise behavioral control in Matlab. J Neurosci Methods 2008; 174: 245–58.

Carr ZJ, Torjman MC, Manu K, Dy G, Goldberg ME. Spatial memory using active allothetic place avoidance in adult rats after isoflurane anesthesia: a potential model for postoperative cognitive dysfunction. J Neurosurg Anesthesiol 2011; 23: 138–45.

Cibelli M, Fidalgo AR, Terrando N, Ma D, Monaco C, Feldmann M, et al. Role of interleukin-1beta in postoperative cognitive dysfunction. Ann Neurol 2010; 68: 360–8.

de Lafuente V, Romo R. Neuronal correlates of subjective sensory experience. Nat Neurosci 2005; 8: 1698–703.

de Lafuente V, Romo R. Neural correlate of subjective sensory experience gradually builds up across cortical areas. Proc Natl Acad Sci U S A 2006; 103: 14266–71.

Gabbott PL, Rolls ET. Increased neuronal firing in resting and sleep in areas of the macaque medial prefrontal cortex. Eur J Neurosci 2013; 37: 1737–46.

Garbarini F, Cecchetti L, Bruno V, Mastropasqua A, Fossataro C, Massazza G, et al. To move or not to move? Functional role of ventral premotor cortex in motor monitoring during limb immobilization. Cereb Cortex 2019; 29: 273–82.

Gervasoni D, Lin SC, Ribeiro S, Soares ES, Pantoja J, Nicolelis MA. Global forebrain dynamics predict rat behavioral states and their transitions. J Neurosci 2004; 24: 11137–47.

Gugino LD, Chabot RJ, Prichep LS, John ER, Formanek V, Aglio LS. Quantitative EEG changes associated with loss and return of consciousness in healthy adult volunteers anaesthetized with propofol or sevoflurane. Br J Anaesth 2001; 87: 421–8.

Hudson AE, Calderon DP, Pfaff DW, Proekt A. Recovery of consciousness is mediated by a network of discrete metastable activity states. Proc Natl Acad Sci U S A 2014; 111: 9283–8.

Ishizawa Y, Ahmed OJ, Patel SR, Gale JT, Sierra-Mercado D, Brown EN, et al. Dynamics of propofol-induced loss of consciousness across primate neocortex. J Neurosci 2016; 36: 7718–26.

John ER. The neurophysics of consciousness. Brain Res Rev 2002; 39: 1–28.

Kelz MB, Sun Y, Chen J, Cheng Meng Q, Moore JT, Veasey SC, et al. An essential role for orexins in emergence from general anesthesia. Proc Natl Acad Sci U S A 2008; 105: 1309–14.

Kline RP, Pirraglia E, Cheng H, De Santi S, Li Y, Haile M, et al. Surgery and brain atrophy in cognitively normal elderly subjects and subjects diagnosed with mild cognitive impairment. Anesthesiology 2012; 116: 603–12.

Krzisch M, Sultan S, Sandell J, Demeter K, Vutskits L, Toni N. Propofol anesthesia impairs the maturation and survival of adult-born hippocampal neurons. Anesthesiology 2013; 118: 602–10.

Kurata K. Corticocortical inputs to the dorsal and ventral aspects of the premotor cortex of macaque monkeys. Neurosci Res 1991; 12: 263–80.

Lemus L, Hernandez A, Romo R. Neural encoding of auditory discrimination in ventral premotor cortex. Proc Natl Acad Sci U S A 2009; 106: 14640–5.

Lepouse C, Lautner CA, Liu L, Gomis P, Leon A. Emergence delirium in adults in the post-anaesthesia care unit. Br J Anaesth 2006; 96: 747–53.

Miyabe-Nishiwaki T, Masui K, Kaneko A, Nishiwaki K, Nishio T, Kanazawa H. Evaluation of the predictive performance of a pharmacokinetic model for propofol in Japanese macaques (Macaca fuscata fuscata). J Vet Pharmacol Ther 2013; 36: 169–73.

Miyabe-Nishiwaki T, Masui K, Kaneko A, Nishiwaki K, Shimbo E, Kanazawa H. Hypnotic effects and pharmacokinetics of a single bolus dose of propofol in Japanese macaques (Macaca fuscata fuscata). Vet Anaesth Analg 2010; 37: 501–10.

Monk TG, Price CC. Postoperative cognitive disorders. Curr Opin Crit Care 2011; 17: 376–81.

Monk TG, Weldon BC, Garvan CW, Dede DE, van der Aa MT, Heilman KM, et al. Predictors of cognitive dysfunction after major noncardiac surgery. Anesthesiology 2008; 108: 18–30.

Pardo-Vazquez JL, Leboran V, Acuna C. Neural correlates of decisions and their outcomes in the ventral premotor cortex. J Neurosci 2008; 28: 12396–408.

Proekt A, Hudson AE. A stochastic basis for neural inertia in emergence from general anaesthesia. Br J Anaesth 2018; 121: 86–94.

Purdon PL, Pierce ET, Mukamel EA, Prerau MJ, Walsh JL, Wong KF, et al. Electroencephalogram signatures of loss and recovery of consciousness from propofol. Proc Natl Acad Sci U S A 2013; 110: E1142–51.

Rizzolatti G, Fogassi L, Gallese V. Motor and cognitive functions of the ventral premotor cortex. Curr Opin Neurobiol 2002; 12: 149–54.

Romo R, de Lafuente V. Conversion of sensory signals into perceptual decisions. Prog Neurobiol 2013; 103: 41–75.

Sepulveda POt, Carrasco E, Tapia LF, Ramos M, Cruz F, Conget P, et al. Evidence of hysteresis in propofol pharmacodynamics. Anaesthesia 2018; 73: 40–8.

Shirasaka T, Yonaha T, Onizuka S, Tsuneyoshi I. Effects of orexin-A on propofol anesthesia in rats. J Anesth 2011; 25: 65–71.

Steinmetz J, Christensen KB, Lund T, Lohse N, Rasmussen LS. Long-term consequences of postoperative cognitive dysfunction. Anesthesiology 2009; 110: 548–55.

Stratmann G, Sall JW, Bell JS, Alvi RS, May L, Ku B, et al. Isoflurane does not affect brain cell death, hippocampal neurogenesis, or long-term neurocognitive outcome in aged rats. Anesthesiology 2010; 112: 305–15.

Tanne-Gariepy J, Rouiller EM, Boussaoud D. Parietal inputs to dorsal versus ventral premotor areas in the macaque monkey: evidence for largely segregated visuomotor pathways. Exp Brain Res 2002; 145: 91–103.

Vlajkovic GP, Sindjelic RP. Emergence delirium in children: many questions, few answers. Anesth Analg 2007; 104: 84–91.

Witlox J, Eurelings LS, de Jonghe JF, Kalisvaart KJ, Eikelenboom P, van Gool WA. Delirium in elderly patients and the risk of post-discharge mortality, institutionalization, and dementia: a meta-analysis. JAMA 2010; 304: 443–51.

Wong KF, Smith AC, Pierce ET, Harrell PG, Walsh JL, Salazar AF, et al. Bayesian analysis of trinomial data in behavioral experiments and its application to human studies of general anesthesia. In: Conference Proceedings: Annual International Conference of the IEEE Engineering in Medicine and Biology Society IEEE Engineering in Medicine and Biology Society Conference 2011; 2011. p. 4705–8.

Wong KF, Smith AC, Pierce ET, Harrell PG, Walsh JL, Salazar-Gomez AF, et al. Statistical modeling of behavioral dynamics during propofol-induced loss of consciousness. J Neurosci Methods 2014; 227: 65–74.